SEISMIC PERFORMANCE OF TALL REINFORCED CONCRETE PIERS WITH HOLLOW SECTIONS

(Translation from Proceedings of JSCE ,No.613/V-42,103-120,February 1999)

Yasuyuki YUKAWA

Tatsuo OGATA

Kumiko SUDA

Hajime SAITO

In order to investigate the seismic performance of tall reinforced concrete piers with hollow sections, cyclic loading tests were conducted using 15 specimens at 1/10 scale. Reinforcement arrangements in the scale specimens were very similar to those of real piers. In the tests, the effects of the following factors were studied: (1) arrangement and amount of transverse reinforcement; (2) range of reinforcement; (3) shape of section at pier bottom; (4) shear span ratio; and (5) torsion. Through this study, it is found that the designed ductility could be guaranteed by arranging transverse reinforcement according to the latest design code. In addition, structural details of a suitable reinforcement arrangement are proposed based on the test results. Finally, measures for predicting ductility and hysteresis damping are developed.

Key Words: *reinforced concrete, high pier, hollow section, re-bar arrangement method, ductility*

Yasuyuki Yukawa is an examiner chief in the Tokushima Construction Office at Japan Highway Public Corporation, Tokushima, Japan. He is a member of JSCE.

Tatsuo Ogata is an acting chief in the Bridge and Structural Engineering Division at Japan Highway Public Corporation, Tokyo, Japan. He is a member of JSCE.

Kumiko Suda is a senior research engineer in the Kajima Technical Research Institute, Tokyo, Japan. She obtained her D.Engineer from the University of Tokyo in 1999. She is a member of JSCE.

Hajime Saito is a research engineer in the Kajima Technical Research Institute. He is a member of JSCE.

---

1. INTRODUCTION

A number of plans exist for the construction of rigid-frame bridges with high piers over 30 m tall, including those along expressways such as the Second Tomei Expressway, which will pass through several mountain ranges. Tall reinforced concrete (RC) piers usually have hollow sections in order to reduce their own weight. However, axial compression stress at the bottom of a pier is about 3 to 5 N/mm^2, which is over three times higher than that in ordinary piers. In the case of a rigid-frame structure, a torsional force acts onto the piers when a seismic force perpendicular to the bridge axis causes horizontal deformation of the main girder. Because there is a relationship between torsional and bending stiffness, the ratio of torsional moment to bending moment increases as the piers become taller. There are many cases where this ratio has reached 10% to 20% at the bottom of piers in elastic response analysis of rigid-frame bridges with high piers. These structural characteristics of high piers are unfavourable from a viewpoint of seismic performance. Thus, it is important to fully understand the seismic performance of high RC piers with hollow sections in order to assure seismic safety.

Experimental studies on RC hollow piers and comparisons with solid ones have been relatively few. Experiments by Kawashima[1] on RC piers with circular hollow sections, and those by Ishii et al.[2] on steel reinforced concrete (SRC) piers are among the notable examples. Kawashima[1] performed reversed cyclic loading tests on RC piers with circular solid and hollow sections for comparison. The reinforcement arrangement consisted of one layer of longitudinal steel bars around the perimeter of a cross section. The study demonstrated that in hollow sections, the cover concrete spalls easily on the inner surface because it is unconfined. The study concluded that excessively thin cover concrete may lead to shear failure, and thus should be avoided. On the other hand, Ishii et al.[2] performed reversed loading tests on SRC piers with solid sections, SRC piers with hollow sections, and RC piers with hollow sections, in order to check differences in seismic resistance of SRC piers with solid and hollow sections. Both SRC and RC specimens had one layer of longitudinal reinforcement around the perimeter of the cross section. The results indicated that ductility factors for hollow sections were lower than those for solid ones. Based on these past studies, it is clear that hollow section piers are less ductile than solid piers, the reason being their vulnerability to spalling of the cover concrete on the inner surface of hollow sections.

After the Great Hanshin-Awaji Earthquake Disaster, numerous design and construction manuals[3),4)] were revised to include tie arrangements as a requirement. However, there have only been a few experimental studies on actual tie arrangements so far, and further work is necessary as regards this issue. On the other hand, tall piers usually require large cross sections of several meters, and the wall thickness may reach 1 m. Reinforcement is usually arranged in the longitudinal direction in one or two layers, near the inner and outer surfaces of the wall. Experimental studies by Miyamoto et al.[5] and Shimbo et al.[6] both considered the features of practical tie arrangements.

Miyamoto et al.[5] performed tests using specimens with circular hollow sections provided with one layer of reinforcement at the inner and outer surfaces, and with various wall thicknesses and amounts of ties. The tests were performed to investigate the effect of differences in the ratio of shear to flexural strength on the ductility of the member. The results confirmed a correlation between this strength ratio and ductility, as already accepted in the case of members with solid rectangular sections. Shimbo et al.[6] investigated the effects of different tie arrangements on the ductility of RC columns with hollow sections in a study on main tower members subjected to large axial loads. Specimens had two layers of longitudinal reinforcement, one each at the inner and outer surfaces of the wall. Comparisons were carried out between specimens without any ties, and those with ties worked in different patterns. The test results confirmed that ductility is improved if hoops at the inner and outer surfaces are confined using intermediate ties, or if the longitudinal reinforcement at the outer surface and hoops at the inner surface are confined with intermediate ties.

Shearing deformation is usually ignored in evaluating the ductility of piers with solid sections. Egawa et al.[7] performed incremental reversed loading tests on beams with solid and hollow sections. Their study revealed that shearing stress is greater in hollow sections than in solid sections. These larger shearing stresses, in turn,

caused the following problems in members with hollow sections: diagonal cracks developed from the onset of the test; the ultimate displacement and absorbed energy decreased slightly; the shear reinforcement strain was greater for a given displacement; and the ratio of shearing deformation to total deformation increased as the shear span ratio decreased. On the other hand, the effect of shearing deformation on piers with hollow sections has not yet been investigated, and the applicability of the evaluation method for pier ductility used with solid sections to those with hollow sections is uncertain.
Shimbo et al.[8] also studied the effect of torsional loading. However, no study has clarified how compatibility torsion affects the ductility of members.
In other words, there has been no experimental study on RC high piers with hollow sections so far which has clarified their ductility in consideration of actual arrangements of transverse reinforcement. Furthermore, the amount of experimental data concerning the effects of ties on ductility is not yet sufficient.
In this study, cyclic loading tests using 1/10 scale models of high piers with various reinforcement arrangements were conducted. An outline of the tests (section 2) and their results (sections 3 and 4) are given in the paper. Furthermore, the effects of transverse reinforcement on ultimate displacement (section 5), and hysteresis damping of RC members with hollow sections (section 6) are discussed on the basis of the test results. Finally, detailed structural specifications for RC high piers with hollow sections are proposed (section 7), taking into consideration the results and information obtained through the study.

2. OUTLINE OF TESTS

Here, an outline is given of the loading tests using 1/10 scale models of typical tall piers designed for highway bridges. "Typical" refers to tall piers with a height (H) of 40m, a breadth of cross section (b) of 6m, a height of cross section (h) of 6m, a wall thickness (t) of 1m with D51 longitudinal reinforcement placed at a pitch of 150mm, longitudinal reinforcement consisting of 0.02-0.03bh, hoops amounting to 0.003-0.004ba (a: hoop interval), and a average volumetric ratio (ρ_{sh}) of transverse reinforcement between 1.00% and 1.50%.

2.1 Specimens

One-tenth scale models of typical tall piers were prepared for the test (H=3.3 m; b=0.6 m; h=0.6 m; t=0.1 m; longitudinal reinforcement (D6) 27 mm apart; longitudinal reinforcement of 0.02 bh; hoops of 0.0019 to 0.0063 ba; and average volumetric ratio of transverse reinforcement 0.75% to 2.44 %).

2.1.1 Details of Specimens

Table 1 gives details of each specimen and its reinforcement arrangement. In the tests, specimen No. 1 was assumed to be a standard specimen. Variations among specimens were related to the following parameters: (i) amount of transverse reinforcement, namely the hoops and ties (Nos. 2, 3, 4, 5, and 16); (ii) tie arrangement (Nos. 6,7, and 8); (iii) diameter of ties (No. 9); (iv) range of reinforcement provided with ties (No. 13); (v) configuration of cross section at pier base (Nos. 10 and 11); (vi) shear span ratio (No. 12); and (vii) whether torsional force was applied or not (No. 14).

2.1.2 Configuration and Materials of Specimens

Figure 1 shows a layout of specimen No.1. For longitudinal and transverse reinforcement, D6 bars and deformed 4-mm and 3-mm bars were used in accordance with the reduced scale of the cross section. Figure 2 shows examples of stress-strain relationships of reinforcing bars used for the test, and Table 2 shows their yield and tensile strength.
High-performance non-compaction concrete was used for the specimens, because the wall thickness was extremely thin (at 100 mm) and the cover and reinforcement interval were only several millimeters. The maximum aggregate size was 10 mm. Compression strength of the concrete was between 38 and 42 N/mm^2 and its modulus of elasticity was between 25 and 29 kN/mm^2 at the time of the tests.

Table 1 Details of Specimens

Specimen No.	Transverse reinforcement								Cross Section at the bottom	Loading	
	Hoops			Intermediate ties							
	Interval (mm)	Type of bars	Amount of hoops	Intervals (mm)	Horizontal interval, d (mm)	Type of bars	Pattern	Area of Reinforcement		Shear span ratio	Torsion
1	35	D4	0.0036*ba*	35	96	D4	A	Full height	Hollow	5	-
2	30		0.0042*ba*	30							
3	20		0.0063*ba*	20							
4	35		0.0036*ba*	35	187						
5				35	54						
6				70	187		B				
7				35	96		C				
8					98		D				
9					54	D3	A				
10					96	D4			Solid (1*h*)		
11					187						
12					96				Hollow	2.5	
13								1*h*			
14								Full height		5	Present
15	65		0.0019*ba*	65							-

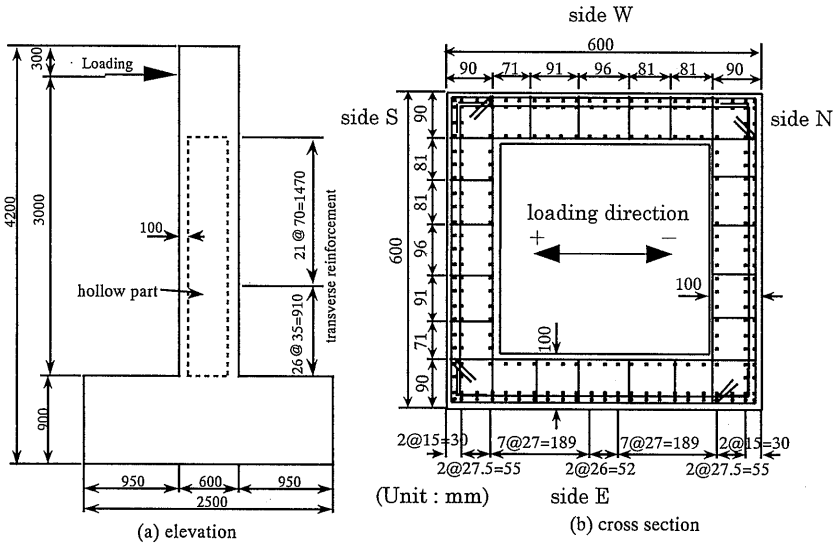

Figure 1 Layout of Standard (No.1) Specimen

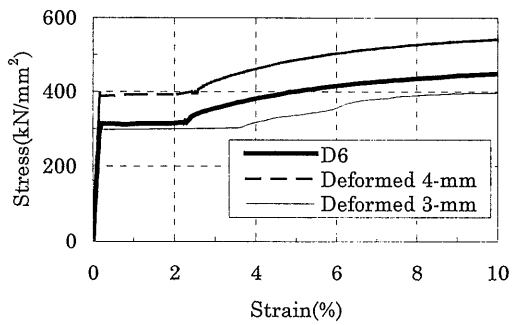

Figure 2 Stress-Strain Relationship of Reinforcing Bars

Table 2 Strength of Reinforcing bars

Type of bars	Yield strength (kN/mm²)	Tensile strength (kN/mm²)
D6	320	469
Deformed 4-mm	397	573
Deformed 3-mm	308	406

The transverse reinforcement was arranged as shown in Table 1 from the bottom of the column to 1.5 h (900 mm) in all the specimens except for specimen No.14 which was subjected to torsional force. Above a height of 1.5 h, the transverse reinforcement interval was doubled.
Four different patterns of intermediate ties were selected as test parameters, as shown in Figure 3. Type A is a standard pattern where 180° hooks (with an anchorage length of 12 d, where d is the reinforcement diameter) are provided on the outer surface and standard 90° hooks (anchorage length: 12 d) are provided on the inner surface of the cross section, all of which are hooked to the hoops. Type B is a pattern conventionally used for spacing bars, in which both ends are bent as standard 90° hooks (anchorage length: 12 d) and hooked to the longitudinal reinforcement. Type C is a pattern similar to type B, but the ends are hooked to the hoops. Type D has no hooks on the outer ends so adequate cover is easily assured, and the anchorage length of the standard 90° hooks on the inner end is rather short at 5 d. Type D was included for the following reasons: because no hooks are provided on the outer end, the intermediate ties would still function as transverse reinforcement even when the outer cover concrete spalls; and because the ties surround the longitudinal reinforcement, it is easier to secure the cover concrete, as compared with types A and C where the ties are hooked onto the hoops. In specimens Nos. 10 and 11 with solid cross sections at the base, intermediate ties of type A were provided in the solid section, and standard 90° and 180° hooks were alternated in a staggered arrangement.

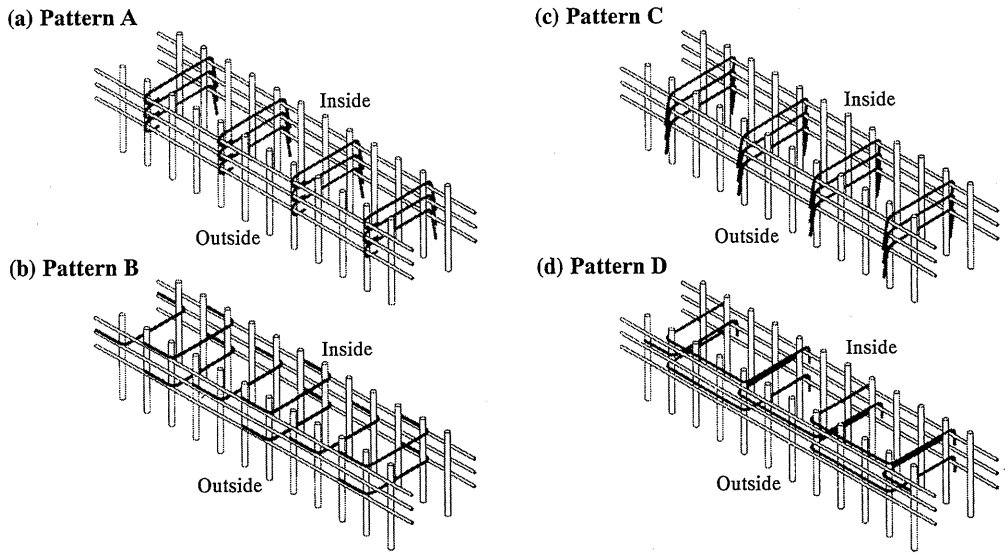

Figure 3 Patterns of Intermediate Ties

2.2.3 Average Volumetric Ratio

In the Specifications for Highway Bridges[4], the volumetric ratio (ρ_s) is defined according to Equation (1) below:

$$\rho_s = \frac{4 A_{sh}}{s\, b_{max}} \tag{1}$$

where b_{max}: effective length of transverse reinforcement (see Figure 4), s: interval of transverse reinforcement, A_{sh}: cross-sectional area of transverse reinforcement

Further, the Specifications for Highway Bridges specify the maximum interval for

intermediate ties on the assumption that hoops and intermediate ties have the same diameter. As such, the test results would be impossible to compare if intervals between transverse reinforcement vary significantly within a cross section, or if the diameters of hoops and ties differ. In this work, the intervals between intermediate ties within a cross section and the diameter of the reinforcement are chosen as test parameters.

For this reason, the average volumetric ratio (ρ_{sh}) was adopted as an index for the amount of transverse reinforcement, since this reflects differences in the two parameters mentioned above. The average volumetric ratio here is treated as the ratio between the total volume of transverse reinforcement (Vsh) underneath the compressive flange (reinforcement shown by dotted lines in Figure 5) and the total volume of concrete (Vch) confined within the reinforcement underneath the compressive flange (the region indicated by hatched lines in Figure 5).

$$\rho_{sh}=\frac{V_{sh}}{V_{ch}}=\frac{A_{sh}\,L_{sh}}{b_c\,t_c\,s} \qquad (2)$$

where L_{sh}: total length of transverse reinforcement underneath the compressive flange, b_c, t_c: refer to Figure 5.

Table 3 compares the volumetric ratio (ρ_s) obtained as per the Specifications for Highway Bridges and the average volumetric ratio (ρ_{sh}).

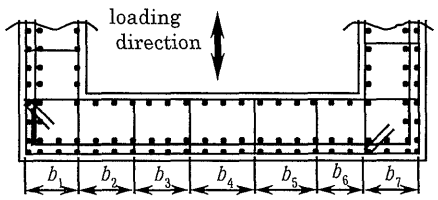

b_{max} = maximum value of b_1–b_7

Figure 4 Calculation Procedure of the Volumetric Ratio

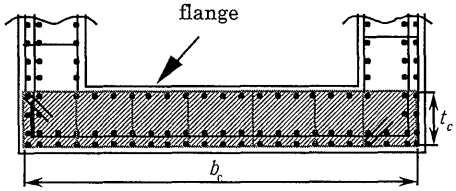

Figure 5 Calculation Procedure of the Average Volumetric Ratio

Table 3 Comparison with the Volumetric Ratio to the Average Volumetric Ratio

Specimen No.	ρ_s (%)	ρ_{sh} (%)
1	1.00	1.39
2	1.16	1.62
3	1.75	2.44
4	0.51	1.27
5	1.20	1.58
6	0.34	1.15
7	0.34	1.15
8	0.98	1.45
9	0.67	1.39
10	1.00	1.39
11	0.51	1.27
12	1.00	1.39
13	1.00	1.39
14	1.00	1.39
15	0.54	0.75

2.2 Methods of loading

2.2.1 Reversed Cyclic Horizontal Loading

For the specimens subjected to reversed cyclic horizontal load (Nos. 1 to 13 and 15), hydraulic tandem jack capable of both forward and backward motions with a capacity of 980 kN was used for horizontal reversed loading.

At the same time, axial loading was provided by a 980 kN hydraulic jack mounted on a loading frame via a horizontal sliding apparatus, so as to exert a downward constant vertical compression load. This axial load was controlled to maintain a constant value of 588 kN. (The average compression stress in concrete in the hollow sections was 2.94 N/mm^2.)

Loading was controlled based on the value 178.4 kN, which is the design yield load

(the load which causes yielding of the tensile reinforcement core as assumed in design) obtained in the calculation of RC sections for standard specimen No. 1. Specifically, the load increment was kept at about 30 kN (for reversed loading) until the design yield load was reached; thereafter, displacement was controlled (for 3 cycle reversed cyclic loading) to be a multiple of the horizontal displacement observed when the design yield load was reached (design yield displacement Δ=11.3 mm).

For specimens Nos. 2 to 11, 13, and 15, controlled loading was applied as in the case of specimen No. 1 until the displacement reached Δ=11.3 mm, and thereafter reversed cyclic loading was applied for 3 cycles so as to maintain the displacement at a multiple of the value Δ=11.3 mm mentioned above.

For specimen No. 12, the value of $\Delta$was set at 3.8 mm based on the design yield load of 359 kN, which differs from the rest of the specimens because the shear span ratio of this specimen is different. Loads were applied in the same manner as for No. 1 specimen, with 3 cycles of reversed cyclic loading to induce displacement in multiples of the value Δ=3.8 mm.

2.2.2 Reversed Cyclic Loading with Horizontal and Torsional Loads

In the case where reversed horizontal and torsional loads were applied (specimen No. 14), two 980 kN hydraulic tandem jacks positioned horizontally were used alternately, with the load applied via loading blocks positioned at the top of the specimen. The total load applied by the two jacks equals the horizontal load, while the difference in the loads multiplied by the distance between the two jacks equals the torsional moment. Axial force was applied by a 1,960 kN center-hole hydraulic jack via an unbonded prestressing strand passing through the specimen. As in the other specimens not subjected to torsional forces, the axial load was controlled to be constant at 588 kN. (The average compression stress of concrete in the hollow section was 2.94 N/mm^2.) The additional bending moment induced by the axial load was taken into account by calculation.

For control of torsional loading, it was assumed that compatibility torsion occurred in typical tall piers. Thus, until the crack-inducing load is reached, the loading was controlled so as to maintain a constant ratio of 15 % between the torsional moment and bending moment at the column base, using as a reference the upper limit values obtained in elastic response analysis of bridges with high piers. After cracks developed, loading was controlled to maintain the same ratio between the torsional and bending deformations as before the onset of cracks. Since it was confirmed that deformation prior to cracking was close to the above-mentioned elastic response analysis, torsional deformation was controlled using the deformation ratio given by Equation (3) based on the calculation results.

$$\frac{\dfrac{\textit{rotational angle at load application point}}{\textit{height from pier base}}}{\textit{horizontal displacement at load application point}} = 73{,}300\ \textit{rad/m}^2 \qquad (3)$$

This load control method was applied to the horizontal load until a value Δ= 11.3 mm was reached, as with the other specimens. Thereafter, displacement control was applied for 3 cycles of reversed cyclic loading, maintaining the displacement at a multiple of the value ofΔ.

2.3 Method of Measurement

Measurements were taken for loading, displacement, and strain. Cracks were visually inspected. Load cells attached to jacks were used to measure horizontal and axial loads. In addition to measuring the horizontal displacement at the load application points for the purpose of load control, measurements were also taken for horizontal displacement distribution in columns, average curvature at the column base, shearing deformation, and torsional angle (for specimen No. 14 only).

For curvature (ϕ), measuring frames were installed at 250 mm and 600 mm from the top face of the footing and the vertical displacement was measured at 4 locations

around the frames. Using the measured values, the average curvature for each section between the frames was calculated using Equation (4).

$$\phi = \frac{\frac{(I_i + II_i)}{2} - \frac{(III_i + IV_i)}{2}}{Y} \quad (4)$$

Here, refer to Figure 6 for I_i through IV_i, Y, and y.

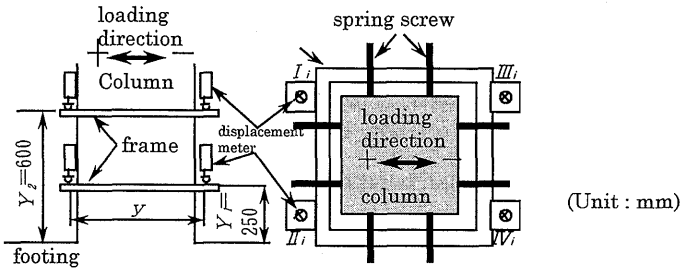

(a) elevation (b) cross section

Figure 6 Details of Curvature Measuring

For shearing deformation, ring displacement meters were attached between the measuring frames on the footing and at locations 250 mm and 600 mm from the footing as shown in Figure 7, so the meters and frames intersect. The measured displacements were used to obtain shearing deformation in a particular section based on Equation (5).

$$\text{Shearing deformation} = \frac{(V_i - VI_i)}{2} \times Cos\ \alpha_i \quad (5)$$

Here, refer to Figure 7 for V_i, VI_i, and α_i.

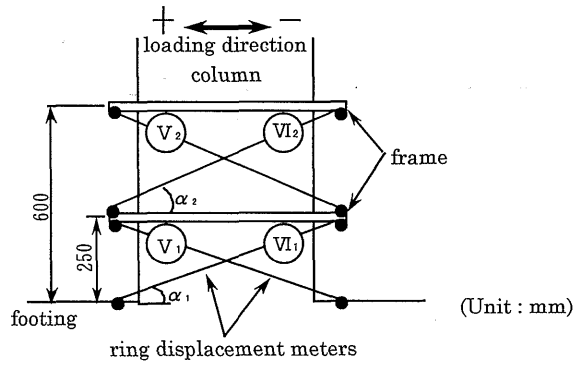

Figure 7 Details of Measuring of Shearing Deformation

Strain gauges were used to measure strain in the longitudinal reinforcement, hoops, intermediate ties, and concrete. Cracks were inspected visually.

3. TEST RESULTS

3.1 Load-Displacement Relationship and Failure Process

The load-displacement relationship and failure process for each specimen are

described in this section. Here, the displacement observed at the design yield load set for the standard specimen was assumed to be the design yield displacement (Δ), and failure process of specimens is discussed on the basis of plasticity ratios derived from the value Δ. The "ultimate state" is defined here as the point at which the envelope of the load-displacement curve falls below the design yield load.

Table 4 shows the failure process for each specimen, Figure 8 shows predicted failure process diagrams for standard specimen No. 1. Figure 9 shows the load-displacement relationship for each specimen, and Figure 10 shows the crack distribution in each specimen in the ultimate state. The numerals given for plasticity ratios in Table 4 indicate that the particular phenomenon occurred under a displacement-controlled load that maximizes the plasticity ratio. On the other hand, observations were not made within the columns during loading. Thus the predictions made in the failure process diagrams are based on measurements of reinforcement strain and the results of observing column sections cut at a height of 600 mm (1 h) from the top surface of the footing after termination of loading.

Table 4 Failure Process for Each Specimen

Event / No.	Maximum Load		Outer cover concrete				Intermediate ties		Longitudinal reinforcing bar			
			Spalling at corners		Spalling widely		Hook angle becoming loose		Buckling		Breaking	
1	+4Δ	-4Δ	+6Δ	-6Δ	+8Δ	-8Δ	+10Δ	−9Δ	+9Δ	-9Δ	+10Δ	-10Δ
2	+5Δ	-5Δ	+6Δ	-7Δ	+8Δ	-9Δ	+10Δ	-10Δ	+9Δ	-9Δ	+11Δ	-10Δ
3	+4Δ	-4Δ	+7Δ	-7Δ	+9Δ	-9Δ	+13Δ	-12Δ	+11Δ	-11Δ	+12Δ	-11Δ
4	+4Δ	-4Δ	+6Δ	-6Δ	+6Δ	-6Δ	+7Δ	-8Δ	+6Δ	-8Δ	+10Δ	-9Δ
5	+4Δ	-4Δ	+6Δ	-6Δ	+8Δ	-8Δ	+11Δ	-11Δ	+9Δ	-9Δ	+10Δ	-11Δ
6	+5Δ	-5Δ	+5Δ	-5Δ	+7Δ	-7Δ	+8Δ	-8Δ	+7Δ	-7Δ	+10Δ	-10Δ
7	+5Δ	-5Δ	+6Δ	-6Δ	+7Δ	-7Δ	+8Δ	-8Δ	+7Δ	-7Δ	+10Δ	-10Δ
8	+5Δ	-5Δ	+6Δ	-6Δ	+7Δ	-7Δ	—	—	+7Δ	-7Δ	+9Δ	-9Δ
9	+5Δ	-5Δ	+7Δ	-6Δ	+9Δ	-8Δ	+10Δ	-10Δ	+9Δ	-9Δ	+10Δ	-11Δ
10	+3Δ	-3Δ	+6Δ	-6Δ	+7Δ	-7Δ	+7Δ	-8Δ	+7Δ	-8Δ	+9Δ	-9Δ
11	+4Δ	-4Δ	+6Δ	-5Δ	+6Δ	-6Δ	+7Δ	-6Δ	+7Δ	-6Δ	+9Δ	-9Δ
12	+5Δ	-5Δ	+9Δ	-9Δ	+10Δ	-10Δ	+11Δ	-11Δ	+10Δ	-10Δ	—	—
13	+4Δ	-4Δ	+7Δ	-7Δ	+7Δ	-7Δ	+9Δ	-9Δ	+7Δ	-8Δ	+10Δ	-10Δ
14	+5Δ	-5Δ	+7Δ	-8Δ	+8Δ	-8Δ	+9Δ	-9Δ	+9Δ	-9Δ	+11Δ	—
15	+4Δ	-4Δ	+6Δ	-6Δ	+6Δ	-6Δ	+8Δ	-8Δ	+6Δ	-6Δ	—	-9Δ

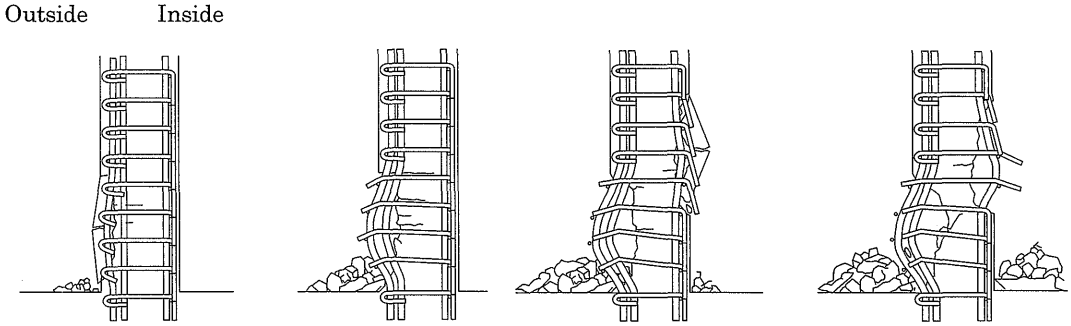

Spalling of outer cover
Buckling of outer re-bar

(a) Predicted ±8Δ

Dropping away
of outer cover

(b) Predicted ±10Δ
(1st cycle)

Buckling of inner re-bar

(c) Predicted ±10Δ
(3rd cycle)

Crushing of outer
core concrete

(d) Failure state
after examination

Figure 8 Predicted Failure Process Diagrams for Standard (No.1) Specimen

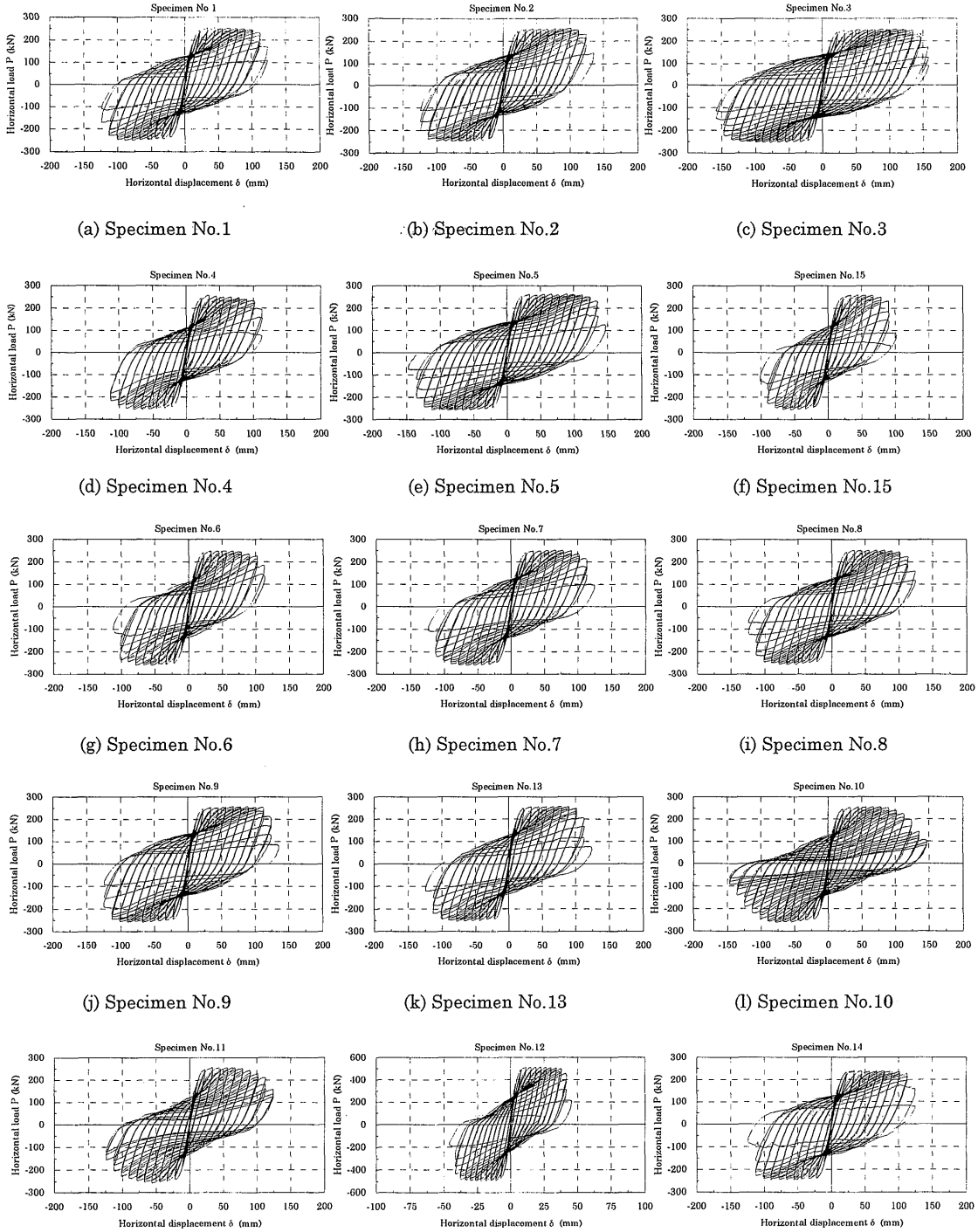

(a) Specimen No.1 (b) Specimen No.2 (c) Specimen No.3

(d) Specimen No.4 (e) Specimen No.5 (f) Specimen No.15

(g) Specimen No.6 (h) Specimen No.7 (i) Specimen No.8

(j) Specimen No.9 (k) Specimen No.13 (l) Specimen No.10

(m) Specimen No.11 (n) Specimen No.12 (o) Specimen No.14

Figure 9 Load-Displacement Relationship for each Specimen

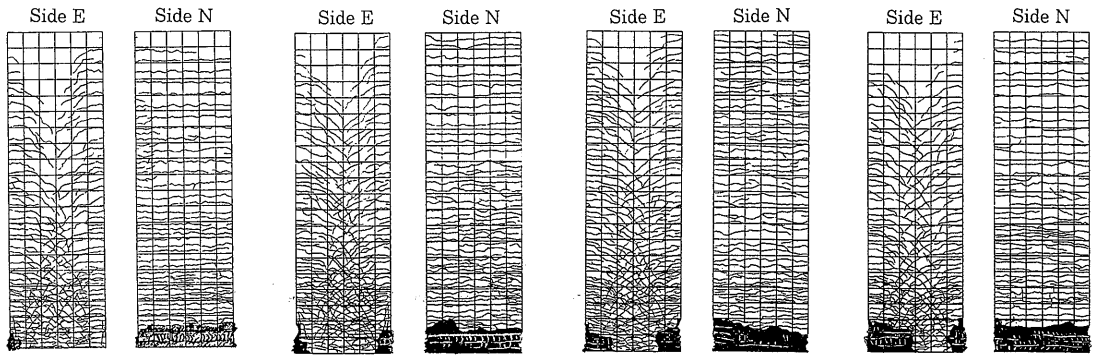

(a) Specimen No.1 (10 Δ)

(b) Specimen No.2 (11 Δ)

(c) Specimen No.3 (14 Δ)

(d) Specimen No.4 (10 Δ)

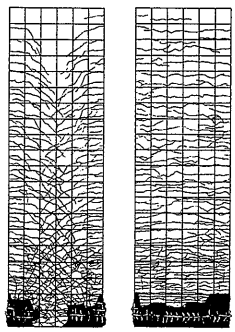

(e) Specimen No.5 (13 Δ)

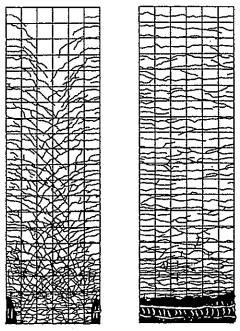

(f) Specimen No.15 (8 Δ)

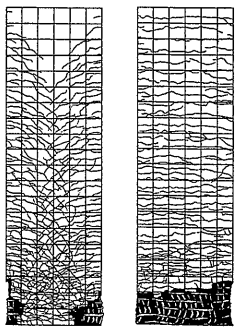

(g) Specimen No.6 (10 Δ)

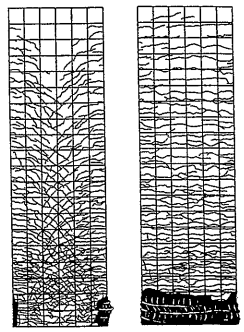

(h) Specimen No.7 (10 Δ)

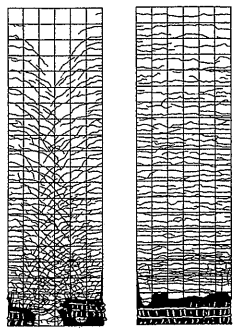

(i) Specimen No.8 (11 Δ)

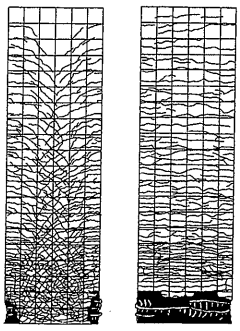

(j) Specimen No.9 (11 Δ)

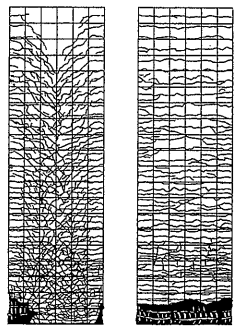

(k) Specimen No.13 (10 Δ)

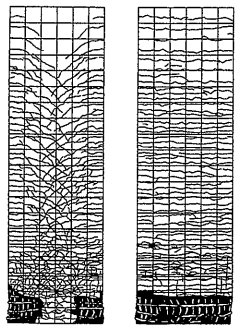

(l) Specimen No.10 (12 Δ)

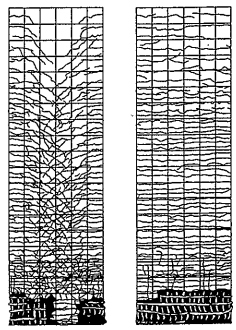

(m) Specimen No.11 (11 Δ)

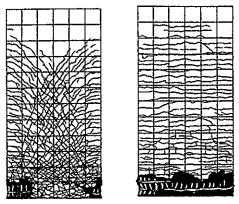

(n) Specimen No.12 (11 Δ)

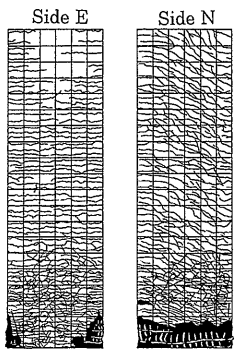

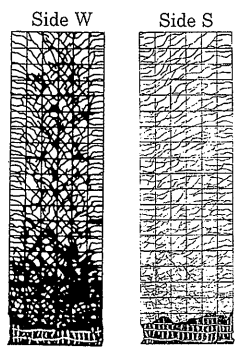

(o) Specimen No.14 (11 Δ)

Figure 10 Crack Distribution in each Specimen

3.1.1 Failure Mode of the Standard Specimen

The standard specimen (No. 1) failed by the following process:
(i) the maximum load was reached at around ±3Δ, and was maintained until roughly ±9Δ;
(ii) cover concrete spalled at corners at around ±6Δ, and the longitudinal reinforcement at corners began to buckle locally in the small interval (35 mm) between hoops;
(iii) cover concrete over the flange partially spalled and dropped away at ±8Δ, and local buckling of longitudinal reinforcement was observed in the flange section as well, in the small interval (35 mm) between hoops (see Figure 8(a));
(iv) at ±9Δ, standard 180° hooks on the outer end, which had been hooked to hoops in the first layer, started to come loose.
Spalling of cover concrete over the flange section became more extensive (reaching the area in the vicinity of 15 cm of the top surface of the footing), and buckling of the longitudinal reinforcement was observed;
(v) in the first cycle of loading at ±10Δ, the load fell from that at ±9Δ, and the load decreased more conspicuously as cycling progressed. In addition, it was confirmed that the standard 180° hooks of intermediate ties that had been hooked to the second layer of hoops began to loosen outward (see Figure 8(b));
(vi) in the first cycle of loading at +10Δ, longitudinal reinforcement at a corner failed, and in the third cycle of loading at -10Δ, longitudinal reinforcement in other regions failed. These failures were confirmed visually, although no crackling noise accompanying failure was heard in either case. Failures were observed in reinforcement that had buckled locally in the small intervals (35 mm) between hoops. Failure is believed to have been caused by bending in the reverse direction to the buckling due to the cyclic loading mode(see Figure 8(c)); and
(vii) although the test was terminated at -11Δ when the residual strength had fallen below 45 % of the maximum load, the axial load was maintained throughout the test.
The terminal condition of failure was as shown in Figure 8 (d).
The standard specimen exhibited excellent ductility. Thus, it seems that aseismic design should be possible for typical high piers while taking into consideration ductile capacity, if the reinforcement arrangement is such that bending failure is allowed to occur first.

3.1.2 Specimens with Varying Amounts of Lateral Reinforcement

Specimens No. 2 through 5 and 15 are variations with features related to the amount of transverse reinforcement.
The failure process of No. 2 specimen was almost the same as that of the standard specimen. While the load on No. 1 began to decrease at ±10Δ , the decrease with the No. 2 began at ±11Δ.
In a slight difference from Nos. 1 and 2, the longitudinal reinforcement of No. 3 specimen began to rupture at corner, before the standard 180° hooks of intermediate ties began loosening outward. The load began to decrease at ±13Δ.
In specimen No. 4, spalling of the cover concrete and buckling of the longitudinal reinforcement began at ±6Δ, slightly earlier than with the standard specimen. The load started decreasing at ±9Δ.
Unlike Nos. 1 and 4, the longitudinal reinforcement in the flange section of No. 5 began to rupture before the standard 180° hooks of intermediate ties began to loosen outward. The failure process was almost the same as that of No. 3. The load began to decrease at ±11Δ.
In specimen No. 15, the standard 180° hooks of intermediate ties began to loosen outward, the longitudinal reinforcement started buckling, and the load began to fall at ±8Δ. Thereafter, the longitudinal reinforcement failed at ±9Δ.

3.1.3 Specimens with Varying Intermediate Tie Arrangements

Specimens No. 6 through 8 are variations with features related to the arrangement

of intermediate ties.
In specimen No. 6, the longitudinal reinforcement buckled at ±7Δ, and the hooks of intermediate ties loosened outward at ±8Δ. Thereafter, the load began to decrease at ±9Δ, and the longitudinal reinforcement failed at ±10Δ. At this point, cover concrete crushed and was unable to withstand the axial loads any longer, thus the test was terminated.
Specimen No. 7 underwent a failure process similar to that of the specimen No. 6, but was able to sustain the axial load in the ultimate state.
The load began to decrease at ±9Δ.
With specimen No. 8, the longitudinal reinforcement buckled at ±7Δ, and the reinforcement failed and the load began to decrease at ±9Δ.

3.1.4 Specimens with Varying Diameters of Intermediate Ties

For specimen No. 9, the average volumetric ratio was the same as in specimen No. 1, and deformed 3-mm steel bars, which are smaller in diameter, were used as intermediate ties. This specimen underwent a failure process similar to that of No. 1. The load began to decrease at ±11Δ.

3.1.5 Specimen with Varying Range of Reinforcement by Intermediate Ties

Specimen No. 13 was provided with intermediate ties only in the region up to a height of 1 h from the pier base. This specimen underwent a failure process similar to the standard specimen. The load began to decrease at ±9Δ.

3.1.6 Specimens with Varying Cross Section Configurations at Pier Base

The cross section up to a height of 1 h above the pier base was solid in specimens Nos. 10 and 11. The amount of transverse reinforcement in these specimens was equivalent to that in specimens Nos. 1 and 4, respectively.
With specimen No. 10, the standard 90° hooks of intermediate ties began to loosen outward and the longitudinal reinforcement started buckling at ± 7Δ. Thereafter, the standard 180° hooks of intermediate ties loosened outward, the longitudinal reinforcement failed, and the load began to decrease at ±9Δ.
With this specimen, the standard 90° hooks of intermediate ties are located on the outer surface. As such, these hooks began to loosen outward and the longitudinal reinforcement started buckling earlier than in the case of specimen No. 1.
In the case of specimen No. 11, the standard 90° hooks of intermediate ties began to loosen outward and longitudinal reinforcement started buckling at ± 6Δ. Thereafter, the standard 180° hooks of intermediate ties loosened outward, the longitudinal reinforcement failed, and the load began to decrease, at ±8Δ.

3.1.7 Specimen with Varying Shear Span Ratios

Specimen No. 12 had a shear span ratio of 2.5, which is smaller than the rest of the specimens. This specimen underwent a failure process similar to that of the standard specimen. The load began to decrease at ±11Δ.

3.1.8 Specimen with Varying Torsional Load

Specimen No. 14 was subjected to reversed horizontal and torsional loads. Figure 9 (o) shows results after subtracting the horizontal load corresponding to the additional bending moment induced by the axial load, so as to enable comparison with other specimens.
Concrete spalled most conspicuously at the corners of one side (side W) where the shearing stresses induced by both horizontal and torsional loads were combined at ±8Δ. Thereafter, the standard 180° hooks of intermediate ties began to loosen outward at ±9Δ and the load started decreasing at ±10Δ.

3.2 Ductility Factor

In the model tests performed for the study, reinforcing bars of radii corresponding to the reduced scale of the outer dimensions of the cross section were used. Hence, the displacement ductility factor μ_δ and curvature ductility factor μ_ϕ were calculated based on actual measurements of horizontal displacement and average curvature at the base, including rotational displacement caused by pulling-out of the bars.

Here, μ_δ and μ_ϕ are defined as shown in Equations (6) and (7), respectively, based on the load-displacement relationship. This way, differences among the specimens in the strength and modulus of elasticity of concrete, as well as in the amount of transverse reinforcement, are reflected.

$$\mu_\delta = \frac{\delta_u}{\delta_y} \tag{6}$$

$$\mu_\phi = \frac{\phi_u}{\phi_y} \tag{7}$$

where δ_y: measured horizontal displacement under load when the strain induced in the outermost longitudinal tensile reinforcement reaches the yield strain (the yielding load), δ_u: measured horizontal displacement when the load falls to the yield load after passing the maximum load, ϕ_y: measured average curvature at time specified for δ_y, ϕ_u: measured average curvature at time specified for δ_u

Here, the curvature indicates the average value of those taken for a section up to 25 cm from the footing surface. For specimens No. 1 through 3 and 6, however, measurements were not taken for the average curvatures in the 25-cm long section. Thus, average curvatures for the section up to 60 cm (1 h) from the footing surface are shown in parentheses for reference. Table 5 shows the values of μ_δ and μ_ϕ for each specimen, and Figure 11 shows the relationship between μ_δ and μ_ϕ Within the scope of the tests, the values of curvature ductility factor were within a range approximately 1.5 to 2.5 times those of displacement ductility factor, even though some deviations were observed.

Table 5 Values of μ_δ and μ_ϕ for Each Specimen

Specimen No.	Yield state			Ultimate state		Maximum Load	Displace-ment ductility factor	Curvature ductility factor
	Load P_y (kN)	Displacement δ_y (mm)	Curvature ϕ_y (/m)	Displacement δ_u (mm)	Curvature ϕ_u (/m)	P_{max} (kN)	μ_δ	μ_ϕ
1	188.5	12.9	(0.00455)	115.5	(0.05888)	252.4	9.0	(12.9)
2	189.1	12.9	(0.00382)	129.1	(0.06506)	255.0	10.0	(17.0)
3	187.5	12.8	(0.00463)	154.1	(0.07772)	247.4	12.0	(16.8)
4	194.0	13.1	0.00718	113.4	0.10973	252.4	8.6	15.3
5	191.4	12.1	0.00677	139.3	0.14075	257.6	11.5	20.8
6	196.0	13.0	(0.00473)	109.8	(0.05719)	248.1	8.4	(12.1)
7	194.0	12.9	0.00699	114.6	0.11284	249.8	8.9	16.1
8	192.1	12.4	0.00637	117.8	0.11785	251.9	9.5	18.5
9	194.4	12.8	0.00707	125.1	0.12117	256.0	9.8	17.1
10	189.5	12.0	0.00623	126.3	0.13925	254.2	10.5	22.4
11	191.1	12.0	0.00650	116.0	0.12961	254.6	9.6	19.9
12	381.5	4.5	0.00616	42.7	0.08613	510.7	9.5	14.0
13	191.1	12.3	0.00534	113.1	0.11017	257.7	9.2	20.6
14	190.8	13.8	0.00678	119.0	0.10019	236.0	8.6	14.8
15	193.1	11.0	0.00578	93.4	0.09097	258.4	8.5	15.7

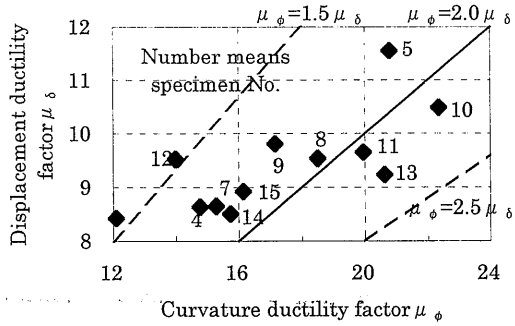

Figure 11 Relationship between μ_δ and μ_ϕ

4. DISCUSSION OF TEST RESULTS

4.1 Effects of Transverse Reinforcement Arrangement

4.1.1 Hoop Interval and Intermediate Tie Interval within a Cross Section

In order to change the values of ρ_{sh}, the hoop interval may be varied (specimens No. 1, 2, 3, and 15; those shown by ■ and ● in Figure 12 with a regression line as a dotted line), or the intermediate tie interval within a cross section may be varied (specimens No. 1, 4, and 5; those shown by ■ and ○ in Figure 12 with a regression line as a solid line). Figure 12 shows the relationship between displacement ductility factor (μ_δ) and ρ_{sh} for specimens with various hoop intervals and intermediate tie intervals within a cross section (specimens No. 1, 2, 3, 4, 5, and 15). Within the scope of the tests, a larger effect on μ_δ was observed when the intermediate tie interval was varied (the solid line in Figure 12) than when the hoop interval was varied (the dotted line in Figure 12).

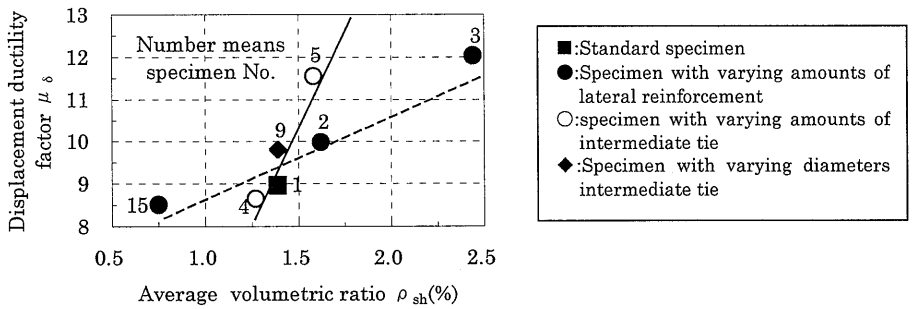

Figure 12 Relationship between Displacement Ductility Factor (μ_δ) and ρ_{sh}

4.1.2 Arrangement of Intermediate Ties

Since the tests were performed using specimens under an axial compression stress of about 3 N/mm^2 and with sufficient shear reinforcement, the results were comparable in the range of high displacement ductility factors. Although differences in the intermediate tie arrangement did not affect the displacement ductility factors significantly, the effect of tie arrangement is discussed below in terms of differences in failure behavior.

In type A (specimen No. 1), where standard 180° hooks were used throughout for intermediate ties on the outer surface, the ties functioned as designed in constraining the core concrete and suppressing buckling of the longitudinal reinforcement, even when the cover concrete began to spall. When the spalling became more severe and the tips of hook anchorages were exposed, the hook angle became loose and tie functionality of was degraded.

In type B (specimen No. 6), where connection to the longitudinal reinforcement

was only provided at the inner and outer surfaces of the cross section, intermediate ties did not serve their function at all. The longitudinal reinforcement buckled over an extensive area as soon as the cover concrete began to spall. After buckling, the core concrete spalled badly in flange areas, and finally the test was terminated when the specimen was unable to withstand the axial load any longer.

In type C (specimen No. 7), the standard 90° hooks began to loosen as soon as the cover concrete spalled, and the ties lost their functionality as described above.

In type D (specimen No. 8), where the anchorage length of the inner standard 90° hooks was about five times the bar diameter (for types A through C, the length was 12 times the bar diameters), the displacement ductility factor was about the same as with type A. Intermediate ties served their function regardless of changes in conditions such as cover concrete spalling, because they were not provided with outer hooks. When the deformation became extensive and concrete spalling progressed in the flange section, however, local buckling often occurred in the small intervals between longitudinal reinforcement surrounded by the ties, because the reinforcement was tightened by the ties.

Based on these observations, it is confirmed that in types B and C the transverse reinforcement did not function for the most part, and in types A and D similar effects were observed with respect to the ties. In type D, in particular, the intermediate ties functioned as designed regardless of cover concrete spalling, because there were no outer hooks.

4.1.3 Diameter of Intermediate Ties

Specimen No. 9 had the same value of ρ_{sh} as specimen No. 1, and the radius of the intermediate ties was made smaller. Test results for the specimen No. 9 are also indicated in Figure 12 (by the ◆ symbols). The value of μ_δ for specimen No. 9 was slightly larger than that for specimen No. 1 (shown by ■). In terms of the effect of transverse reinforcement on suppression of longitudinal reinforcement buckling, the diameter of the ties need not be the same as the hoops, if the principle is observed that restraint spring provided by transverse reinforcement is determined based on the bending stiffness of the hoops and the axial stiffness of the ties[9]. Furthermore, if the relationship described above between hoop interval and intermediate tie interval within a cross section is also taken into consideration, the test results are believed to suggest that use of more reinforcing bars of smaller diameter as ties would effectively enhance their functionality.

4.1.4 Range of Reinforcement Provided with Intermediate Ties

In order to clarify the effect of differences in the range over which intermediate ties, are provided specimens No. 1 and 13 were compared for the distribution of cracks as shown in Figure 13, and for the load-plasticity ratio relationship as shown in Figure 14. Plasticity ratio μ_r is given by Equation (8) as follows:

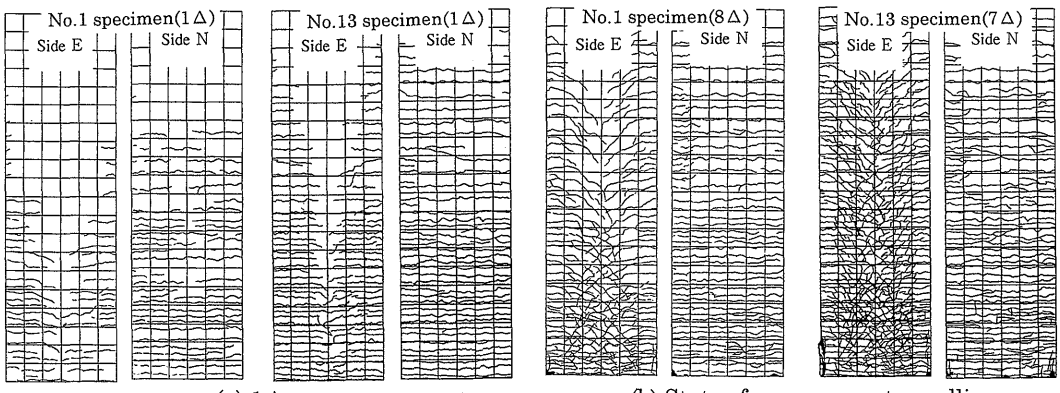

(a) 1Δ (b) State of cover concrete spalling

Figure 13 Comparison with Specimens No. 1 to 13 for Distribution of Cracks

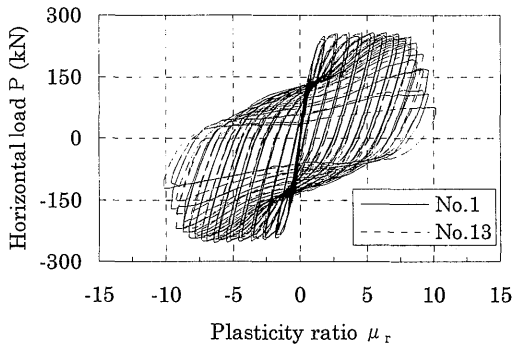

Figure 14 Load-Plasticity Ratio Relationship for Specimen No.1 and No.13

μ_r = horizontal displacement (δ) / δ_y (8)

In specimen No. 13, the region above height 1 h from the base was not even provided with spacing bars. As such, slightly more cracks were observed for this specimen as compared with standard specimen. However, the ductility was equal to or greater than that for standard specimen. Thus, it was concluded that in cases similar to the high piers studied here, where columns have been securely reinforced against shear and where bending failure is concentrated at the pier base, a ductility similar to that of columns fully provided with intermediate ties can be maintained even if the columns have been provided with ties only up to 1 h from the base.

4.2 Effect of Cross-Sectional Configuration at Pier Base

Figure 15 (a) shows the relationship between displacement ductility factor and strength ratio (the ratio between shear strength V and flexural strength Pu) for specimens with a solid cross section at the pier base (Nos. 10 and 11) and those with hollow sections (Nos. 1 and 4) but with the same reinforcement arrangement as the solid specimens. Comparing specimen No. 1 (hollow section) and with No. 10 (solid section at the base), and also No. 4 (hollow section) and No. 11 (solid section at the base), all with the same transverse reinforcement arrangement, the displacement ductility factor was larger for specimens with a solid cross section at the base. However, the relationship between displacement ductility factor and strength ratio, which is a parameter used often for evaluation of ductility factor, reveals that the effect of differences in cross sectional configuration on ductility factor (see arrows in Figure 15 (a)) is small compared to the slope of the line (the broken line in Figure 15 (a)) indicating the relationship for a series of specimens with varying hoop ratios (No. 1, 2, 3, and 15).

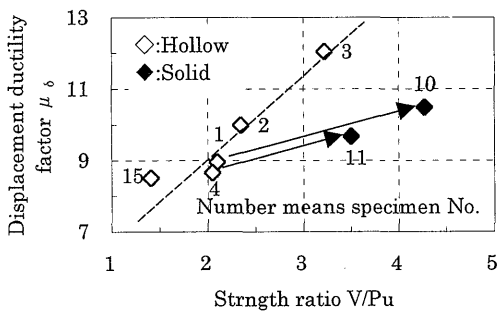

(a)The Ratio between V and Pu

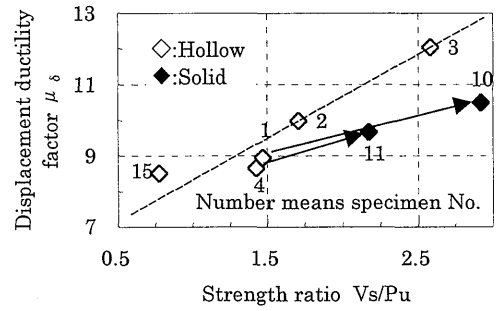

(b) The Ratio between Vs and Pu

Figure 15 Relationship between Displacement Ductility Factor and Strength Ratio

Even when the strength ratio is assessed using the shear capacity provided by the shear reinforcement Vs instead of total shear strength V (Figure 15 (b)), the slopes of the arrows were low compared to that of the broken line. The possible reasons for this include differences in the effect of transverse reinforcement for different cross sectional configurations; in the test, however, intermediate ties were arranged continuously in the solid part and therefore the standard 90° and 180° hooks were placed in a staggered pattern, while the ties in the hollow part were provided with standard 180° hooks on the outer end. As such, the confining effect of intermediate ties was smaller in the solid part, and this may have affected the ductility factor substantially.

4.3 Effect of Loading Conditions

4.3.1 Shear Span Ratio

Figure 16 shows the relationship between plasticity ratio and the ratio of shear deformation to total horizontal displacement at the column capital in the case of specimens No. 1, 10, 12, and 13. Figure 17 shows envelopes of the load-plasticity ratio relationship for these specimens. The shear span ratio for specimen No. 12 was 2.5, and that for all the other specimens was 5.0.
Figure 16 indicates that for the specimens No. 1, 10, and 13, whose shear span ratios were 5.0, the ratio of shear deformation to total horizontal displacement was minimal regardless of the cross-sectional configuration at the base, reaching 2% to 3% at the most. On the other hand, specimen No. 12 with a shear span ratio of 2.5 indicated a shear deformation ratio as high as about 15%. However, Figure 17 reveals that the load-plasticity ratio relationships are almost identical for all specimens with a shear span ratio of 5.0 (No. 1, 10, and 13) and that with a ratio of 2.5 (No. 12), indicating that these specimens have similar ductility. These findings clarify that even though the ratio of shear deformation to bending deformation increases as the shear span ratio decreases, the specimens tested exhibited similar ductility when the amount of transverse reinforcement was the same, although the shear span ratio varied between 2.5 and 5.0.

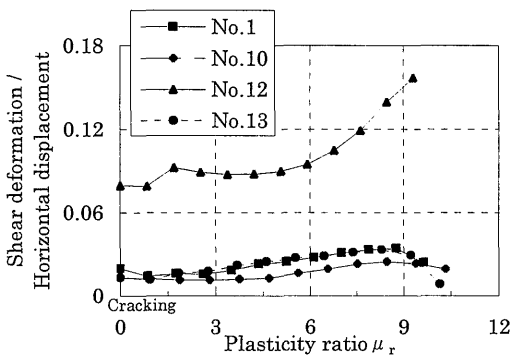

Figure 16 Shear Deformation Ratio

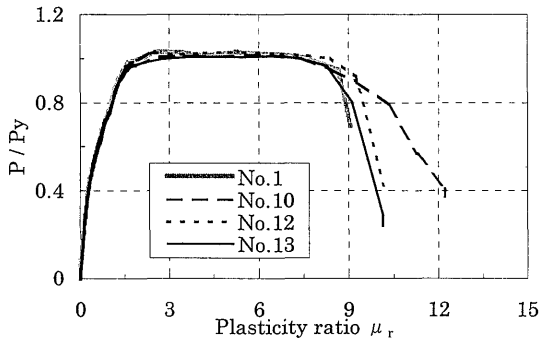

Figure 17 Load-Plasticity Ratio Relationship

4.3.2 Torsional Moment

Using specimen No. 14, ductility under reversed horizontal and torsional loads was investigated, assuming a seismic loading perpendicular to the bridge axis. Figure 18 shows calculated values, which indicate a correlation between bending-torsional failure and shear-torsional failure, as well as the locus of the loads on specimen No.14. For calculation, the methods indicated in the Standard Specifications for Design and Construction of Concrete Structures[3] (the Standards) were used for torsional strength in the absence of shear reinforcement(Tc), shear

strength (Vu), and flexural strength (Mu), and the equation by Hirosawa et al.[10] was used for net shear strength (Tu). Specimen No. 14 was provided throughout with reinforcement arranged in identically to that up to a height 1.5 h from the base of specimen No. 1. This reinforcement arrangement undergoes bending-torsional failure first, even when loaded while maintaining a constant ratio of 15% between the torsional and bending moment. Figure 19 compares the load-plasticity ratio relationship for specimens No. 1 and 14. The maximum load for specimen No. 14 decreased to 95% that for the standard specimen due to the torsional load, but ductility was almost identical. It is possible to quantitatively assess the decrease in maximum load by taking into consideration the relationships shown in Figure 18 during the design process.
Thus, it can be concluded that with respect to compatibility torsion assuming a seismic force perpendicular to the bridge axis, torsional load has a minimal effect on ductility if the ratio between torsional and bending moments under elastic conditions is about 15%, and ductility can be evaluated in the same manner as in a case without the torsional load.

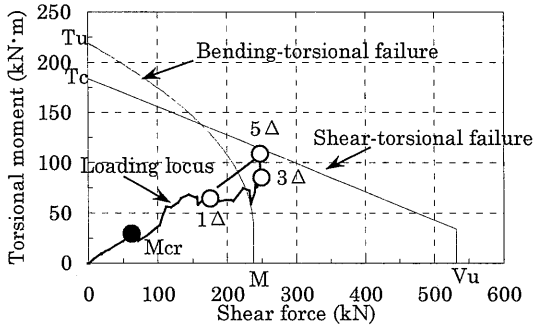

Figure 18 Locus of Loads on Specimen No.14

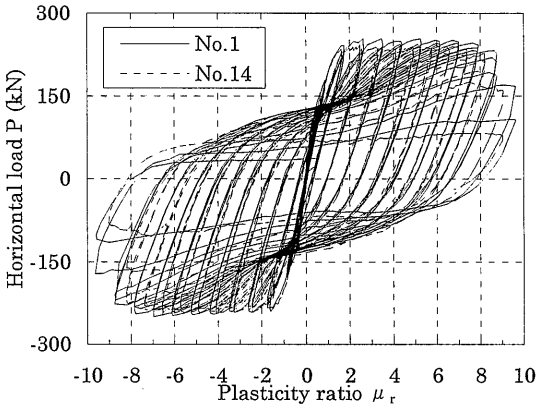

Figure 19 Load-Plasticity Ratio Relationship

5. DISCUSSION OF ULTIMATE DISPLACEMENT

The effect of reinforcement arrangement on the ultimate displacement was studied, on the basis of the test results. Basically, the ultimate displacement was evaluated following the method indicated in the Specifications for Highway Bridges[4]. In these Specifications, the deformation induced by a bending force is calculated based on the M-ϕ relationship. Here, an attempt is made to introduce a parameter that is able to reflect differences in transverse reinforcement arrangement in the stress-strain relationship of confined concrete. In other words, the ultimate strain of concrete corresponding to the test results was derived by an inverse analysis, and its correlation to indices pertaining to the reinforcement arrangement was studied.

5.1 Rotational Deformation at Base

Measured values of horizontal displacement are affected by rotational deformation at the pier base due to pulling-out of the longitudinal reinforcement. Therefore, it is necessary to subtract the deformation component caused by this rotational displacement from the total measured value of horizontal displacement, so as to enable comparison with the calculated value which represents the bending deformation only. For the purposes of study, it was decided to subtract the amount of rotational deformation caused by pulling-out of the longitudinal reinforcement at pier base from the measurement of horizontal displacement. This procedure was adapted because the rotational deformation caused by pulling-out of reinforcement was rather small, since steel bars of relatively small diameter were used as the longitudinal reinforcement.
Angle section was placed on the four corners of the column 30 mm above the top

face of the footing, and the rotational angle about the column base was derived based on the measured relative displacement. The angles thus obtained were multiplied by the value of shear span to obtain the horizontal displacement of the column capital, which in turn corresponds to rotational displacement. The measured relative displacement reflects the pulling-out of reinforcement from the column as well as from the footing, so the rotational deformation caused by pulling-out of the reinforcement may be overestimated. Thus, it should be noted that the amount of deformation at the column capital after subtracting the rotational deformation would be rather small. Since it would be difficult to measure the relative displacement in case where concrete at the pier base spalls, it was decided to estimate the rotational deformation as follows:

(i) measurements are accurate up to a displacement three times the design yield displacement (3Δ), so in such cases the measured value is used as is to calculate the rotational deformation at the base, which in turn is subtracted from the measured horizontal displacement; and

(ii) the values of rotational deformation measured for each specimen are processed by a least squares linear regression, assuming that the amount of deformation corresponding to the angular deformation at the base is directly proportional to the measured horizontal displacement. After reaching 3Δ, the values indicated by a line passing through the values of 3Δ for each of the specimens, that is, with an average gradient of the regression lines for all specimens, are subtracted from the measured horizontal displacement as a component corresponding to rotational deformation at the base.

Table 6 shows the values of yield displacement ($\delta y'$) and ultimate displacement ($\delta u'$) after subtracting this rotational deformation at the base from the measured displacement.

Table 6 Values of $\delta y'$ and $\delta u'$ after Subtracting Rotational Deformation

Specimen No.	Yield state		Ultimate state	
	Load P_y (kN)	Displacement δ_y' (mm)	Load P_u (kN)	Displacement δ_u' (mm)
1	188.5	10.2	188.5	88.4
2	189.1	10.4	189.1	100.4
3	187.5	10.2	187.5	120.3
4	194.0	10.5	194.0	86.9
5	191.4	9.7	191.4	108.4
6	196.0	9.9	196.0	83.8
7	194.0	10.1	194.0	88.5
8	192.1	7.6	192.1	86.9
9	194.4	10.1	194.4	98.4
10	189.5	9.7	189.5	98.1
11	191.1	9.6	191.1	89.3
12	381.5	3.3	381.5	31.7
13	191.1	9.9	191.1	87.9
14	190.8	11.3	190.8	112.1
15	193.1	8.7	193.1	72.1

5.2 Estimation of Ultimate Displacement by Calculation

The method of calculating the ultimate displacement is as follows:

(i) the cross section is divided into 60 equal parts, to clarify the relationship between the moment (M) and curvature (ϕ) of cracked section. The stress-strain relationship for the reinforcement is assumed to be bilinear, and for confined concrete the relationship indicated in the Specifications for Highway Bridges[4] was used. Since this was a model test, the effect of the self-weight of the column specimen was ignored, and the same M-ϕ relationship was assumed throughout the pier in the height direction; and

(ii) the M-ϕ relationship derived in (i) above was assumed to be tri-linear, with

the transition points corresponding to the occurrence of cracking, yielding, and the ultimate state. The load-displacement relationship was derived by double integration of the curvature distribution along the member axis. Here, no plastic hinge was assumed, and the ultimate displacement was calculated based only on the integration of the distribution of ϕ derived from the M-ϕ relationship.

5.3 Discussion of the Stress-Strain Relationship of Confined Concrete

Based on the stress-strain relationship for confined concrete as given in the Specifications[4], a reverse-analysis of the ultimate strain was performed so that the calculated values and test results (δ_u') for the ultimate displacement would be equal. Figure 20 shows the ultimate strain of confined concrete ε_{cu} obtained by the this reverse-analysis. The horizontal axis is an index (x) which incorporates a parameter related to the arrangement of transverse reinforcement. The index x is given by Equation (9).

The parameter x is a non-dimensional value which is a product of the average volumetric ratio, the ratio of the yield strength of the transverse reinforcement and the compression strength of concrete, and a parameter indicating the degree of restraint of the transverse reinforcement.

$$x=100\rho_{sh}\left(\frac{\sigma_{sy}}{\sigma_{ck}}\right)\sqrt{\frac{\frac{d_{tw}}{d_w}}{\frac{l_e}{d_w}-1}} \tag{9}$$

where σ_{sy}: yield strength of transverse reinforcement, σ_{ck}: compression strength of concrete, d_{tw} : diameter of intermediate ties, d_w : diameter of hoops, l_e : effective length of transverse reinforcement

Here, the parameter indicating the intensity of the restraint imposed by the transverse reinforcement was determined in consideration of the fact that a theoretical solution for elastic buckling P_{cr} can be approximated by Equation (10)[11], and the value of β is governed by the axial stiffness of the intermediate ties and the bending stiffness of hoops[9].

$$P_{cr}=C\sqrt{\beta EI} \tag{10}$$

where β : (spring constant of transverse reinforcement) / (interval between transverse reinforcement), C: constant, E: apparent modulus of elasticity of steel bars, I: moment of inertia of steel bars

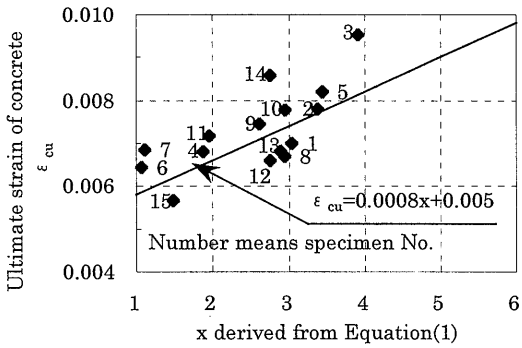

Figure 20 Relationship between ε_{cu} and x

A correlation was observed between the ultimate strain of the confined concrete ε_{cu}, as obtained by the reverse-analysis of ultimate displacement, and the index x, even though the test results fluctuated somewhat. Although a function representing a quadratic curve may be appropriate in a case such as specimen No. 3, the linear equation shown as Equation (11) is adopted for simplicity to calculate the ultimate displacement of each specimen. The results are shown in Figure 21 along with the test results.

$$\varepsilon_{cu}=0.0008x+0.005 \tag{11}$$

The results of calculating the ultimate strain of confined concrete according to Equation (11) were between 0.84 and 1.10 times the test results obtained in the study, indicating a fairly accurate estimate. These results suggest that the index x defined in Equation (9) reflects fairly well the effect of differences in actual arrangement of transverse reinforcement. It should be noted here that Equation (11) is based on the calculation process described in the previous section, and it does not represent the material characteristics of the confined concrete. In other words, Equation (11) cannot be used if the ultimate displacement is derived by a process different from the one described above.

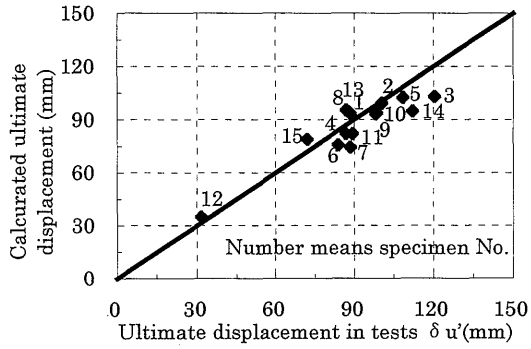

Figure 21 Relationship between Test Results and the Calculated Ultimate Displacement

5.4 Comparison between Tests Results and Calculations According to the Specifications for Highway Bridges

The ultimate displacement of each specimen was calculated as provided for in the Specifications for Highway Bridges[4], and the results are compared in Figure 22 with the test results.

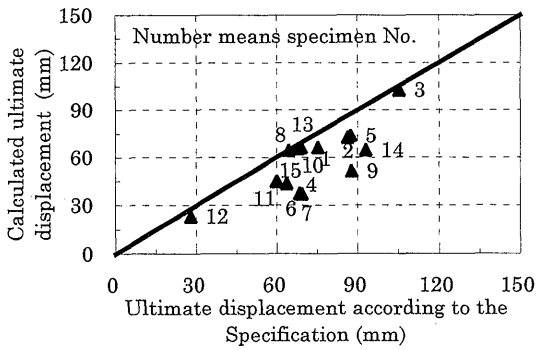

Figure 22 Comparison between Test Results and Calculation according to the Specification

Here, the test results for ultimate displacement indicated on the horizontal axis

are the points where horizontal strength, which was stable in the vicinity of the maximum horizontal strength begins falling, as specified in the Specifications for Highway Bridges. In the model tests, the displacement is the value observed immediately before decrease in the horizontal load falls by more than 4% of the maximum horizontal strength. (Note that this is different from δ_u'.) Within the scope of the study, the calculation of ultimate strain as given in the Specifications for Highway Bridges yielded values between 0.63 and 1.00 times the test results, so the results are on the safe side. Since there are limits on the choice of arrangement of lateral reinforcement, the results for some of specimens fall excessively on the safe side.

6. DISCUSSION OF HYSTERESIS DAMPING

The behavior of bridges with high piers during earthquakes is quite complex, so the results of non-linear dynamic analysis are often reflected in the design. Here, a hysteresis model of RC members and their damping, as used in non-linear dynamic analysis, are discussed based on the test results.
Hysteresis models commonly used include those configured by Muto et al.[12] and by Takeda et al.[13]. From the viewpoint of unloading stiffness, the model by Muto et al. can be described as origin-oriented, up to the yielding point after cracks start to develop; beyond yield, the value decreases due to the yield stiffness, and once a point is reached where the bending moment becomes zero, the curve starts rising toward the maximum value of the previous cycle again.
Here, the test results are summarized taking into consideration the P-δ relationship of the entire pier and the M-θ relationship of the plastic hinge section. At the same time, an attempt is made to develop a formula for calculating unloading stiffness, and thus obtain values equivalent to hysteresis damping (equivalent damping factor) as derived from the test results.
Except for the unloading stiffness after yielding, hysteresis rule by Muto et al. is applied.

6.1 Investigation Process

6.1.1 Hysteresis Damping Characteristics of Specimens in Model Tests

Here, the P-δ and M-θ relationships, (of the various hysteresis damping characteristics), are investigated. With respect to the P-δ relationship, the equivalent damping factor was derived for each hysteresis loop according to Equation (12) (see Figure 23), based on the relationship between horizontal load P and measured horizontal displacement δ at the column capital of each specimen.

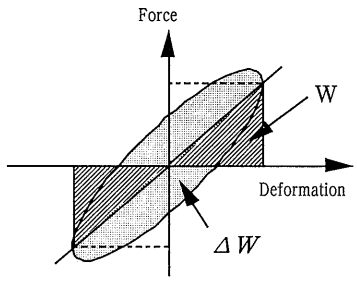

Figure 23 ΔW and W

$$h_{eq}=\frac{1}{2\pi}\cdot\frac{\Delta W}{W} \qquad (12)$$

With respect to the M-θ relationship, the equivalent damping factor was derived for each hysteresis loop as in the case with the P-δ relationship, based on the relationship between bending moment M at the base and average curvature ϕ in the

region up to 25 cm (0.42h) from the base, in order to clarify the hysteresis damping characteristics in the plastic hinge section. The rotational angle θ of the plastic hinge is expressed as a product of ϕ and the length of the hinge. Here, the length of the hinge is assumed to be 25 cm, which is the length of the region measured for average curvature.

6.1.2 Investigation of Unloading Stiffness

The basic hysteresis characteristics, aside from unloading stiffness, were assumed to comply with the hysteresis rules according to Muto et al. By adjusting the values of unloading stiffness, the hysteresis damping characteristics of the analysis model were made equivalent to those in the test results. Specifically, the equivalent damping factor according to the hysteresis rules of Muto et al. is given by Equation (13). Hence, the unloading stiffness k can be expressed as a function of plasticity ratio μ_r and yielding stiffness k_y.

$$h_{eq}=\frac{1}{\pi}\left(1-\frac{k_y}{k}\cdot\frac{1}{\mu_r}\right) \tag{13}$$

6.2 Investigation Results

Figure 24 shows the relationship between equivalent damping factor derived using the P-δ relationship and the displacement plasticity ratio, while Figure 25 shows the relationship between equivalent damping factor derived based on the M-θ relationship and the rotational plasticity ratio. Here, Model A indicates the relationship derived by the method by Muto et al.[12] Model B is a modification of Model A. Unloading stiffness in Model B is given by Equation (14). Model C represents the relationship derived by the method of Takeda et al[13]., and Model D is a modification of Model C (Edo et al.[14]).
Within the scope of the study, the hysteresis models yielded results that correspond well with the test results, although in some cases damping was overestimated, especially when the plasticity ratio was small. The models seem sufficiently accurate for practical application. When the hysteresis rules proposed by Muto et al. are used, the results correspond most closely with the test results under reversed loading, if the unloading stiffness is obtained based on Equation (14), for both P-δ and M-θ relationships.

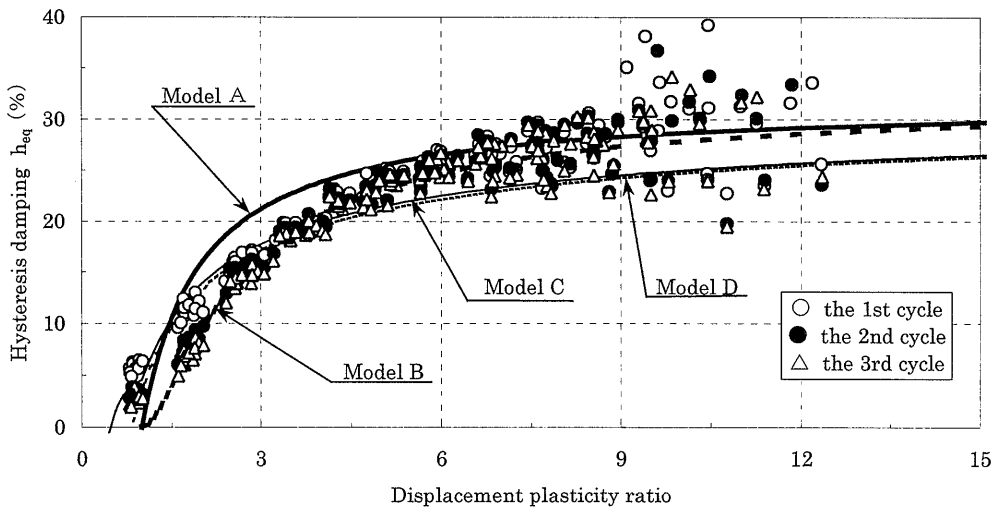

Figure 24 Relationship between h_{eq} Derived from P-δ and Displacement Plasticity Ratio

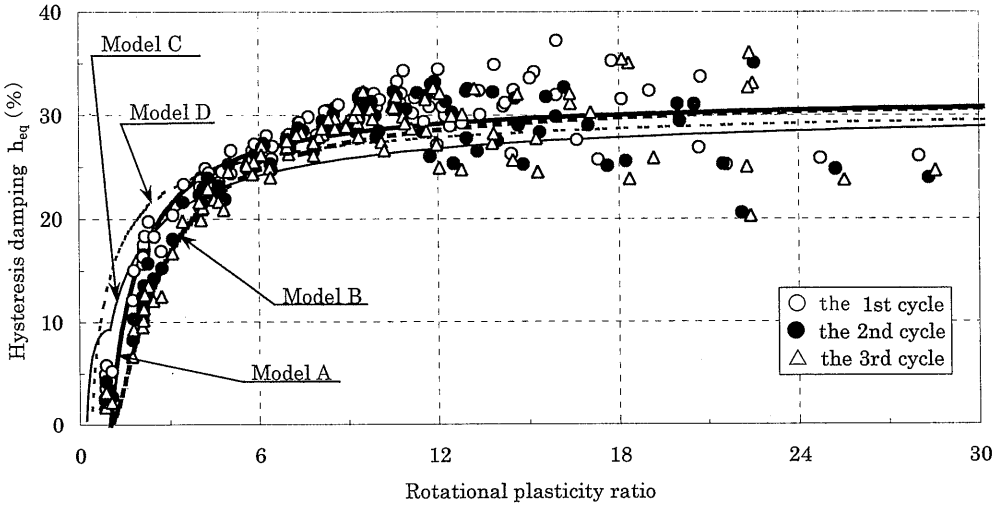

Figure 25 Relationship between h_{eq} Derived from M- ϕ and Rotational Plasticity Ratio

$$k=k_y \cdot \mu_r^{(-1/\mu_r)} \qquad (14)$$

7. PROPOSAL FOR DETAILED SPECIFICATIONS ON REINFORCEMENT FOR TALL RC PIERS WITH HOLLOW SECTIONS

Based on the test results, a proposal is made for detailed specifications on reinforcement for tall RC piers with hollow sections. Since the tests carried out for this study were performed under specific conditions, careful consideration must be made if applying these specifications to cases that deviate significantly from the given test conditions, namely which where: longitudinal reinforcement ratio (value obtained by dividing the total cross sectional area of longitudinal reinforcement by the product of cross sectional area and height of the member) of about 2%; average axial compression stress for concrete used in hollow sections of 2.94 N/mm^2; hoop ratio between 0.2 and 0.6%; average volumetric ratio of lateral reinforcement between 0.7 and 2.6%; shear span ratio between 2.5 and 5.0; and ratio of wall thickness to cross-sectional height of 1/6.

7.1 Extent of Lateral Reinforcement

If sufficient shear reinforcement is provided, and the failure mode is restricted to that induced by bending, a rational reinforcement arrangement can be achieved by providing intermediate ties at locations where bending failures are likely to occur. In the case of tall piers, bending failures occur only at two locations, namely the top and bottom of the pier.
To determine the range over which intermediate ties should be provided, due consideration must be given to the extent of cover concrete spalling. A method has been proposed in which the buckling length of longitudinal reinforcement is used in estimating the spalling area, while at the same time considering the parameters related to the actual arrangement of lateral reinforcement.[9] The estimated range of spalled cover concrete as derived by this method yields values between 1/6 h and 1/3 h, which corresponds well with the test results. The test results indicated that intermediate ties should be provided up to about 1 h from the top and bottom ends of piers to be on the safe side; this corresponds to three to four times the spalled range. Although this can be regarded as a guideline for tall piers, due consideration should be given to particular applications, since spalling increases in range as the diameter of steel bars increases as compared to the cross-sectional dimensions of the pier.

In the model tests, slightly more cracks were observed in ordinary sections without intermediate ties in cases where the ties were provided only at the base. In actual piers, however, spacing bars and other measures are also incorporated, and it is likely that most cracks in ordinary sections will be prevented.

7.2 Arrangement of Intermediate Ties

If intermediate ties are arranged in hollow sections as in type A, it is better to provide standard 180° hooks on the outer ends and provide standard 90° hooks on the inner ends. A Type D arrangement would also exhibit ductility similar to a Type A arrangement, and this has proven advantageous when it is difficult to secure adequate cover due to limitations imposed by wall thickness, etc. As in the test cases where hollow sections are provided with longitudinal reinforcement around the inner and outer surfaces, failure may progress with longitudinal reinforcement on the outer surface buckling first, followed by buckling of that on the inner surface. As such, the anchorage length of standard 90° hooks is sufficient if they can be hooked onto the hoops. In other words, the anchorage length of standard 90° hooks at the inner surface could be reduced as compared with conventional practice. For Type D, the anchorage length of standard 90° hooks around the inner surface is set at five times the diameter, which is necessary to secure they hook onto hoops. In this case, the ductility of the test specimen proved sufficient.

7.3 Diameter of Intermediate Ties

Although applicability is limited to within the scope of these tests, it is possible to use intermediate ties of diameter less than the hoops, as long as the average volumetric ratios are the same.

7.4 Methods of Reinforcement Against Torsion

If there is concern regarding the effect of torsion, a check should be made as to whether bending-torsional failure precedes other types of failure, after due consideration of the correlation between bending-torsional and shear-torsional loads. During design, the bending-torsional strength should be decreased based on the correlation thus observed.

8. CONCLUSION

In tests on tall RC piers with hollow sections, in which reversed cyclic loads modeling assumed seismic loading were applied models that represent actual piers fairly accurately, and in which due consideration was given to of steel bar diameter and arrangement, the following results were obtained:
(i) It was clarified that tall RC piers with hollow sections in general possess excellent ductility;
(ii) An outline of indices useful for evaluating the effects of actual arrangements of intermediate ties on ductility was obtained;
(iii) Detailed specifications for reinforcement were proposed, including arrangements of intermediate ties, their diameter, and methods of reinforcement against torsion; and
(iv) After clarifying the hysteresis damping characteristics of tall RC piers with hollow sections, an equation for evaluating unloading stiffness was proposed and the resulting hysteresis models accurately represent the hysteresis damping characteristics obtained in the tests.

Acknowledgment

The authors are grateful to the members of the study group on aseismic design of bridges with tall piers (organized by the Expressway Technology Center and chaired by Professor Iemura of Kyoto University), Messrs. Tetsuo Matuda and Yasuo Inokuma of Japan Highway Public Corporation, and many others for their valuable advice and generous cooperation.

References

[1] Kawashima,K., "Dynamic Strength and Ductility of Hollow Circular Reinforced Concrete Bridge Pier", Public Works Research Institute, Ministry of Construction, Civil Engineering Journal ,34-10, pp.34-39, 1992. (In Japanese)

[2] Ishii,T., Nakamura,M., Soda,N., "Model Tests on Aseismic Performance of Steel and Reinforced Concrete(SRC) Piers", Nihon Doro Kodan(Japan Highway Public Corporation), Nihon Doro Kodan Research Institute Report, pp.103-114, 1983.11. (In Japanese)

[3] "Japan Society of Civil Engineers(1996) Standard Specifications for Concrete Structure, Seismic Design", JSCE. (In Japanese)

[4] Japan Road Association (1996), Specifications for Highway Bridges Part V: Seismic Design, Japan.

[5] Miyamoto,Y., Ishibashi,T., Saito,T., "Experimental Study on Deformation for Circular Cyrindrical Piers", Proceedings of the 7th JSCE Earthquake Engineering Symposium , pp.1237-1246, 1986. (In Japanese)

[6] Shimbo,H., Murayama,Y., Suda,K., Ichinomiya,T., "Transverse Reinforcement Arrangement Methods to Restrain the Buckling of Longitudinal Bars in Hollow Sectional R/C Piers", Proceedings of JSCE, V-425, pp.850-851, 1995. (In Japanese)

[7] Egawa,N., Iemura,H., Inoue,H., "Experimental Study on Deformation for RC Beem with Hollow Section", Proceedings of the 23rd JSCE Earthquake Engineering Symposium, pp.850-851, 1995. (In Japanese)

[8] Shimbo,H., Murayama,Y., Suda,K., Ichinomiya,T., "Loading Tests of RC Columns by Using Six-Degree -of Freedom Loading Apparatus", Proceeding of JCI, Vol.15, pp.1113-1118, 1993. (In Japanese)

[9] Suda, K., Shimbo, H., Masukawa, J. and Murayama, Y. (1996), "Reinforcing Method to Improve Ductility of RC Column with Hollow Section ", Proceedings of JCI, Vol.18, No.2, pp.725-730, 1996. (In Japanese)

[10] Hirosawa,M., "Past Experimental Results on Reinforced Concrete Shear Walls and Analysis on them", Kenchiku Kenkyu Shiryo, Building Research Institute, Ministry of Construction, March 1975. (In Japanese)

[11] Suda, K., Murayama, Y., Ichinomiya,T. and Shimbo, H. (1994), "Buckling Behavior of Longitudinal Reinforcements in RC Column Subjected to Cyclic Load ", Proceedings of JCI, Vol.16, No.2, pp.467-472. (In Japanese)

[12] Muto, K. (1977), Seismic Design of Structures, Maruzen, Japan. (In Japanese)

[13] Takeda, T., Sozen, M. A. and Nielsen, N. N. (1970), "Reinforced Concrete Response to Simulated Earthquake", ASCE, Vol.96, No.ST12.

[14] Edo,H., Takeda,T., Omote,Y., "Dynamic Loading Tests of Two Stories and One Span R/C Frame (No. 2 , Study of Test Results)", Summaries of Technical Papers of Annual Meeting, Architectural Institute of Japan, Vol. 44th, pp.45-48,1974. (In Japanese)